Influence of Complex External Sound Stimuli on Primary Auditory Cortical Neuron Receptive Fields During Development

A. Sullivan, S. Patil, H. Tieh, S. Vishwakarma

December 14, 2018

Abstract

In the primary auditory cortex (A1), neuronal responses have demonstrated a wide variety of behavior patterns and frequency tunings. Understanding how auditory information is encoded in AI has been thoroughly studied from a mechanistic perspective, but there is limited knowledge about the learning and development of A1 neurons. In this paper, we provide a framework to investigate the impact of a specific auditory stimulus during development on A1 neuronal responses. Using methods including spike triggered analysis, spike triggered covariance, and spike time tiling coefficient, we review neuronal correlations and receptive field properties of A1 neurons in rats reared with a complex sound stimulus. This study demonstrates a complex architectural change in the overall receptive field properties of A1 and suggests neurons became more sharply tuned to the exposure frequency range after complex sound stimulus rearing.

I. Introduction

The primary auditory cortex (A1) serves as the initial processing step for sounds after they are converted to nerve impulses in the cochlea. While the encoding of auditory information in A1 is understood from a mechanistic perspective, much less is known about the learning and development of A1 neurons. It is unclear to what degree the formation of A1 structure and neuronal responses are influenced by external stimuli. Do A1 neurons learn to respond to specific stimuli, or is there a consistent, built-in representation of the frequency space that forms during development? This paper provides a framework to investigate whether the responses of A1 neurons can be altered by presenting a specific auditory stimulus during development such that these neurons exhibit tuning in their receptive fields to characteristics of that stimulus.

II. Background

Receptive fields within primary auditory cortex are ordered topographically according to their preferred frequency tuning, a feature that has been inherited from the cochlea [1]. A1 neuronal responses have demonstrated a wide variety of dynamics, frequency tunings, response thresholds, and patterns of excitatory and inhibitory behaviors. These individual neurons have been extensively studied in murine models using spectro-temporal receptive fields (STRFs) [1]. To delineate the auditory pathway, STRFs are widely used as linear approximations of the signal transform from sound spectrograms to neural responses [2]. STRFs allow a more complete analysis of stimulus-based response properties and auditory processing activity of central auditory neurons to determine the modulation preferences and stimulus selective properties [3]. This method is commonly used to capture time-dependent behavior of spectral profile processing in auditory neurons and show the specificity to cell types (excitatory/inhibitory) as well as laminar position of the cells in the columnar circuit [3].

The neural circuitry in animal brains is constantly undergoing alterations to reflect their changing environments. In the case of the auditory cortex, the brain analyzes auditory stimuli statistics from the environment to modulate its tonotopic map [4]. A large body of literature provides evidence of frequency map plasticity during development in the primary auditory cortex (A1) in numerous animal models—especially in rats [5, 6, 7, 8, 9]. In general, during development, auditory neurons refine their STRF, narrowing their frequency tuning bandwidths (i.e., their tuning specificity) to result in overall smaller

cortical regions devoted to specific tones [8]. Furthermore, lasting A1 cerebral changes induced in critical period tone-reared rats are well documented: critical period rearing on auditory stimuli yields expanded receptive field tuning to the targeted frequencies [10,11]. This overrepresentation of exposure frequencies in the A1 tonotopic map in pulse-tone reared rats demonstrates STRF plasticity in A1 during development [12]. Zhang and collaborators demonstrated monotone pulse-tone exposure in rats during postnatal development yields accelerated A1 tonotopic map formation, as well as expanded A1 representation of the pulse-tone frequency [8]. Compared to naive rats, exposed rats exhibited increased numbers of neurons sharply tuned to characteristic frequencies near that of the exposure stimulus, suggesting further developmental STRF refining near exposure stimulus frequencies [8].

III. Methods

Experimental Design & Data Acquisition

We obtained the data analyzed below from an experimental paradigm designed to probe underlying unsupervised learning dynamics in primary auditory cortex (A1) of rats. Experimenters reared three control rats normally and three experimental rats with a speaker above the home cage continuously playing a complex sound stimulus from 9 days post birth (P9) onwards. The stimulus was composed of two overlapping 5-note chords with a 2-note overlap. The amplitude of each chord was independently chosen every 1/6 of a second. Thus, the stimulus contains both independent components (useful in investigating independent component analysis-based learning) and a correlation structure (useful in investigating Hebbian learning). Figure 1 displays a spectrogram of the exposure stimulus. Note—unlike the following frequency-time plots, the horizontal axis here is frequency (the output from Matlab's spectrogram function).

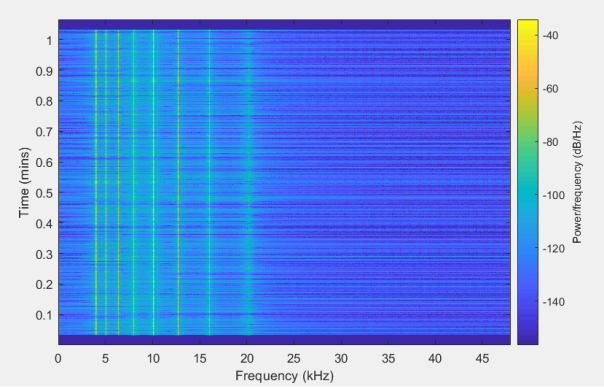

Figure 1: Spectrogram of the complex sound stimulus used to rear experimental mice. Amplitudes of two chords containing five notes each with two overlapping notes were chosen independently every 1/6 of a second.

Auditory activity was recorded at least three weeks after the sound stimulus began (P30), using two silicon multi-electrode probes containing multiple shanks and depths. Spike sorting software was used to extract single unit spikes. Though three different stimuli were used to elicit spiking activity in A1, we only consider the dynamic moving ripple (DMR) stimulus, a 15-minute-long complex sound stimulus used for reverse correlation of receptive fields. Reverse correlation in a causal system takes the time at which a given response of interest is observed, and examines a time window stretching back a fixed time period to identify the cause of this response in stimulus space [13]. In general, the impulse response function of linear-single-input, linear-single-output can be obtained as the cross-correlation function of the response and a white noise input, but the inherent nonlinearity in neural systems makes this simplification rather reductive. Importantly, white noise stimuli are known to cause inhibition of auditory cortical neurons, and thus white noise stimuli must be replaced with an alternative that effectively probes the stimulus-response function [14]. The DMR stimulus envelope is defined by the number of spectral peaks per octave at each time and the instantaneous modulation rate. The DMR envelope is dynamic and structured in both time and

frequency, and short-time spectro-temporal correlations, such as those found in speech or other natural sounds, are present. Ultimately, the DMR stimulus reproduces complex spectro-temporal patterns that are present in natural signals, and are therefore suitable for characterizing the complex STRFs of primary sensory cortical neurons, while simpler probes such as individual tone pips may only uncover a small subset of the receptive field—not taking into account the complex interactions between spectral and temporal stimulus features [14].

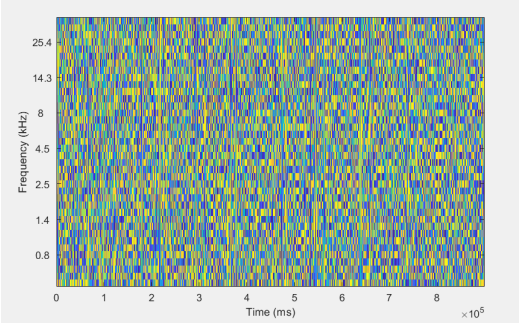

Figure 2: Dynamic moving ripple stimulus spectrogram used for reverse correlation of receptive fields in primary auditory cortex.

Data Analysis

Prior to data analysis, we removed any regions of the provided data structure "e" containing empty arrays of spike times. For example, 2 out of 4 shanks from rat 4 had no data, as did one from rat 2. No other preprocessing was performed.

We primarily employed the spike-triggered average (STA) to approximate the STRF of auditory neurons recorded from A1. In this method, the average of the spike-triggered ensemble, a subset of the entire stimulus, is obtained by extracting a window of fixed temporal length around each detected spike. These spectro-temporal windows are then averaged to obtain a linear filter that approximates the predominant features present prior to all spiking events. For our analyses, we use a window of 250ms (125ms before and 125ms after the spike) over all frequencies present in the DMR stimulus. The STA is defined as follows, where n is the total number of spikes and $\mathbf{x_i}$ is the 250ms window surrounding each spike time in the stimulus spectrogram:

$$STA = \frac{1}{n}\sum_{i=1}^{n} \boldsymbol{x_i}$$

The dominant properties in an STRF can be isolated using a singular-value decomposition approach, in which the STRF matrix (in our case, the STA) is decomposed into a product of 3 matrices, $STRF = USV'$. For the spectro-temporal case, U contains the spectral properties of the receptive field and V the temporal properties; S is a diagonal matrix containing the magnitudes of the singular values associated with each column of U and V. By sorting the singular values in descending order, the most influential spectral and temporal vectors can be obtained and used to approximate the STRF (the ones corresponding to the largest singular value). This separable approximation to the STRF neglects spectro-temporal inseparability but facilitates determining important properties, including peak frequency, peak temporal excitation and inhibition, spectral bandwidths, and temporal durations [15].

Spectro-temporal instability can be a measure of complexity of the STRFs, and often reflects contributions from a slant along the spectro-temporal profile or the presence of multiple excitatory and inhibitory subfields in stimulus space. Here, we characterize spectro-temporal instability as previously done in [16], where the singular values of the STRF, S, are ordered such that the largest is S_1 (in descending order), and so:

$$\alpha_{SVD} = 1 - \frac{S_1^2}{\sum_{i=1}^{N} S_i^2}$$

We also characterize spike train similarities between the experimental and control groups through the spike time tiling coefficient (STTC) [17], a method of spike train correlation analysis that is (relatively) insensitive to firing rate and has been used to examine correlations between spontaneously firing retinal ganglion cells during early development. This parameter calculates neuronal correlations based on the relative fraction of one neuron's spikes that can be explained by the spiking of the other neuron (i.e., if a spike from neuron A falls within some fixed time window—which we take to be 0.1s—of a spike from neuron B, then that spike counts toward the correlation). Though our time window is relatively large, reducing the window by a factor of two further reduces the observed correlations of both distributions. As we are primarily interested in the difference between correlation distributions between the two groups, this should be relatively insensitive to the window size. As evidenced by the STTC formula below, the fraction of spikes of neuron A explained by spikes from neuron B, P_A, and the fraction of B's spikes explained by neuron A, P_B, are determined, along with the total fraction of the recording session (900s) accounted for by the 100ms windows around each spike in A, T_A, and each spike in B, T_B.

$$STTC = \frac{1}{2}\left(\frac{P_A T_B}{1 - P_A T_B} + \frac{P_B T_A}{1 - P_B T_A}\right)$$

A common extension of the spike-triggered average method of receptive field characterization—the spike-triggered covariance (STC)—yields determining multiple filters in stimulus space, rather than the single filter obtained from STA [18]. One obtains the STC by calculating the average covariance of the spike-triggered stimulus ensemble. Finding the eigen-decomposition of the difference between the STC and the covariance of the stimulus itself yields eigenvectors corresponding to the dominant directions in stimulus space in which the covariance of the spike-triggering stimuli is significantly larger or smaller than that of the stimulus itself. Theses dimensions therefore inform which stimulus features the neurons are most sensitive to [19]. STC is defined below, where n is the total number of spikes, STA is the spike-triggered average defined above, and **x** denotes the 250ms window of the stimulus spectrogram around spike **i** [20]:

$$STC = \frac{1}{n}\sum_{i=1}^{n}(\boldsymbol{x_i} - STA)(\boldsymbol{x}_i - STA)^T$$

In conjunction with STA, researchers have employed the STC method to characterize the relevant stimulus subspaces that elicit neuronal spiking in a wide variety of sensory systems, including retinal ganglion cells [21, 22] and primary visual cortex cells [23] in the visual system. STC is significantly more powerful than STA alone, as it permits investigating nonlinear dynamics of neuronal receptive fields [24].

Statistical tests we used here include the Kolmogorov-Smirnov (KS) and Mann-Whitney U (MW) tests for significant differences in the overall distributions from which samples were drawn, and for the medians of these distributions, respectively. We also use the Wilcoxon rank-sum test to evaluate differences in paired samples. When calculated, p values are given, with statistical significance corresponding to $p < 0.05$.

IV. Results

Neuronal Correlations

Prior to determining individual receptive field properties, we hypothesized that recordings from neurons in rats from the experimental population were likely to have an increased degree of correlation in response to the similar features from the exposure stimulus. To test our hypothesis, we utilized a pairwise

correlation metric, the spike time tiling coefficient (STTC) to characterize the correlation between neural spike trains between neurons, a technique intended to be more insensitive to variations in overall firing rate than the "correlation index," an alternative measure of spike train similarity. As we have wide variations in the number of spikes recorded from each neuron—ranging from single spikes to upwards of 3,000 spikes—insensitivity to firing rate is a relevant concern. Even so, our initial STTC analysis revealed a sensitivity to firing rate at very low values (e.g., single spikes), a limitation of the STTC formula above. As discussed later, we decided to restrict our analysis to neurons firing at least 100 spikes in the 15-minute DMR stimulus window to both reduce noise in the calculated STA, and to provide a lower bound on neurons included in our STTC analysis. Figure 3 displays histograms illustrating pairwise correlations of a subset (1.6 million) of experimental neurons and all control neurons, calculated with a correlation time window of 0.1s. We only evaluated pairwise correlations within animals due to computational cost.

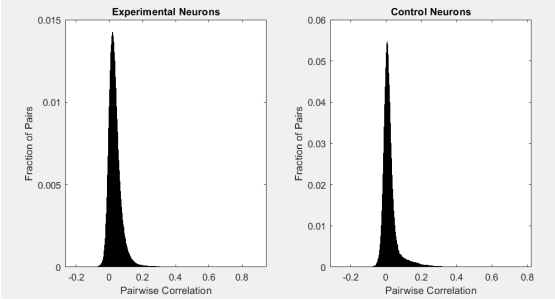

Figure 3: Pairwise correlation distributions from experimental and control neurons.

Both KS and MW tests return p values of 0 for these distributions, indicating an extremely high degree of statistical significance between both the distributions as a whole and their medians. Additionally, both the *mean* (0.0342 vs. 0.0225) and *median* (0.0271 vs. 0.0118) are larger for the experimental neurons, suggesting a higher similarity between spike trains in experimental neurons, which supports our hypothesis of a larger number of neurons responding to similar features from the exposure stimulus. It should be noted that the number of bins is not necessarily equal between the two histograms, as the experimental group had far more data points calculated (1.6 million vs. 247,000) as well as a significantly larger number of recorded neurons. This discrepancy is the likely cause for the pronounced difference in y-axis magnitudes between the graphs in Figure 3, since each bin in the control group accounts for a smaller width of correlation values.

Spike-Triggered Average Characterization

We begin our spike-triggered analysis by characterizing the distribution of receptive field parameters between experimental and control groups. Figure 4a and Figure 4c display two example STAs from the experimental (rat 3, Figure 4a,b) and control (rat 6, Figure 4c,d) groups. Both neurons display a spectro-temporal profile commonly found in auditory neurons containing a sensitive frequency range along the vertical axis, with an excitatory region preceded by an inhibitory region at this sensitive range along the horizontal (temporal) axis. To quantitatively characterize the locations of these sensitive regions, we perform a singular-value decomposition (SVD) to obtain the separable spectral and temporal profiles that yield the best reconstruction of the initial filter (i.e., corresponding to the largest singular value), see Figure 4b and Figure 4d. While these two STAs look similar to those obtained in other primary cortical areas (e.g., auditory cortex), other experiments often show a single large peak and valley along one spectral coordinate (see [15] and [25], for example) rather than the multiple spectral peak configuration shown below. Similar, complex geometries have been obtained for STRFs in ferret A1 [16] and monkey inferior colliculus [26], highlighting an inherent complexity in auditory processing receptive fields.

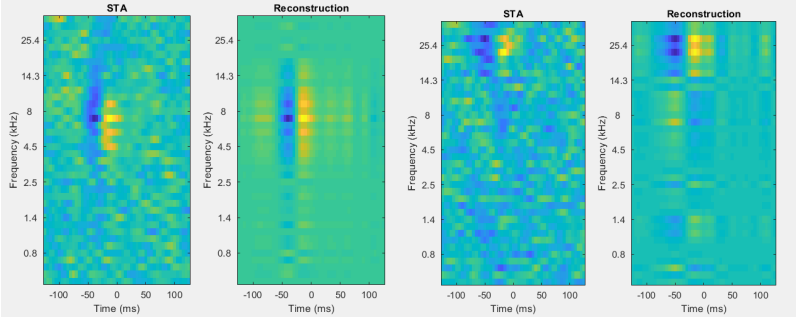

Figure 4: Example spike-triggered averages from neurons from experimental (a,b, left) and control (c,d, right) rats. a and c display calculated STAs from the spectrogram and the recorded spike times. b and d show reconstructions based on the spectral and temporal profiles with the largest singular value from SVD of the STAs, allowing for extraction of the dominant spectral and temporal features the neuron responds to.

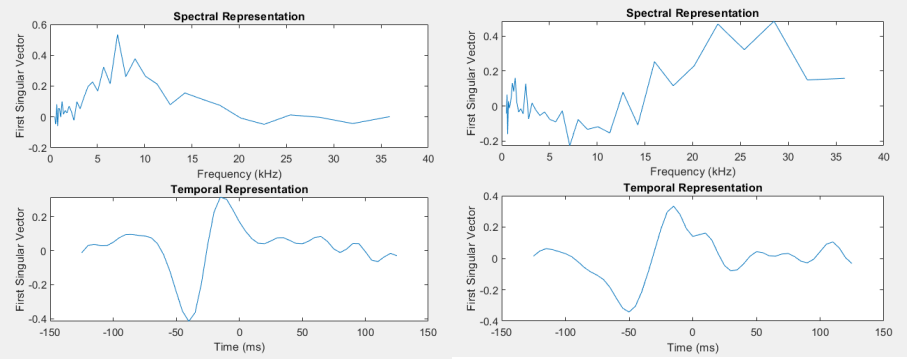

Figure 5: Example spectral and temporal profiles for the two neurons shown above in Figure 4.

The resultant spectral and temporal profiles for the two neurons from Figure 4 are displayed in Figure 5. While the spectral curves are fairly noisy due to the low number of sample points (38), the important features are still easily identifiable and can be extracted without much difficulty. We used a processing script to extract the relevant features for all neurons from the six rats to be compared between conditions, including the vector of spike times (spike train), STA, STC, and eigenvalues and eigenvectors from the difference decomposition between the STC and the stimulus covariance matrix. Furthermore, we extracted the spectral, temporal, and singular value matrices for the STA SVD, as well as a number of other properties extracted from the decompositions. We choose not to examine sign of the effect (i.e., excitatory of inhibitory) at the dominant frequency for each neuron, extracting the frequency with the largest absolute value from the first spectral SVD vector. We also extract the times corresponding to the maximum inhibitory and excitatory temporal effects—constrained to be less than zero, as times after the spike should not have any influence on the probability of spiking. Defining prominent peaks as one with a height of at least 0.2, we then extracted the locations of all prominent peaks in both the spectral and temporal profiles of each STA, identifying prominent peaks from the absolute value of the input vector (Matlab's "findpeaks" function only identifies maxima). Thus, we obtain the height, location, and width of each peak. As the STA is an average of the stimulus window around each spike, accurate determination of the STRF requires enough samples to suppress noise around irrelevant frequencies and times—hence, we restrict our analyses to neurons with at least 100 spikes over the 15-minute window. Figure 6a illustrates an example STA from a neuron with only 52 spikes, clearly exhibiting large amounts of noise with no easily discernable spectro-temporal peaks or valleys. However, even neurons with long spike trains sometimes exhibit STAs with little apparent structure, such as the one in Figure 6b from an experimental cell with 2,366 spikes. We discuss the lack of structure in STAs in the context of STC analysis below.

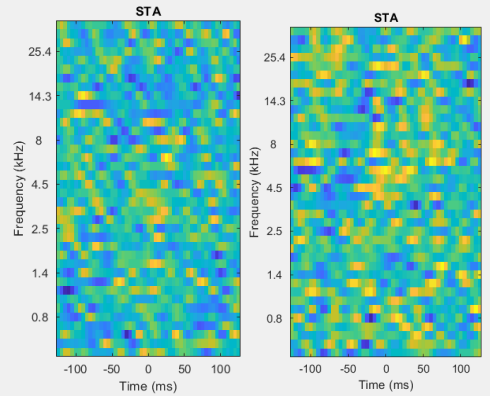

Figure 6: Example STAs for neurons with spike counts under 100 (left) and over 1000 (right). While neurons with counts under 100 often show increased noise in their STAs (left), even neurons with high spike counts can yield STAs without obvious peaks or valleys (right).

Population Analyses of STA Parameters

We begin by considering differences in relevant properties between the entire population of experimental and control rats. Figure 7 displays probability histograms for the maximum sensitive frequency of the control and experimental neuron populations. We hypothesized that more neurons in the experimental group would exhibit receptive fields sensitive to the frequencies present in the exposure stimulus. Summing the fraction of neurons in each bin over the range of the exposure stimuli (the bins containing frequencies from 3.6 to 21.6 kHz) indicates a pronounced difference in the fraction of recorded neurons sensitive to this range of frequencies (0.4610 in the experimental versus 0.3488 in the control). A KS test between the two populations confirms a statistically significant difference in their probability distributions ($p = 3*10^{-5}$), and an MW test rejects the null hypothesis that the medians of the two distributions are equal ($p = 0.0114$). Interestingly, the experimental neurons show a decrease of 0.0824 in the fraction of neurons primarily responsive to frequencies below 3.6 kHz, which accounts for more than half of the 0.1122 increase in the exposure stimulus range. This redistribution between frequencies below the median would not influence the value of the median, suggesting a partial reorganization of the low-frequency end of A1. This is also consistent with the hypothesis that neurons in nearby regions of the A1 tonotopic map will be repurposed to respond to the exposure stimuli. Comparing mean and median of both groups reveals the experimental rats exhibit larger average preferred frequencies than the control, consistent with the repurposing of low-frequency neurons to the exposure stimuli.

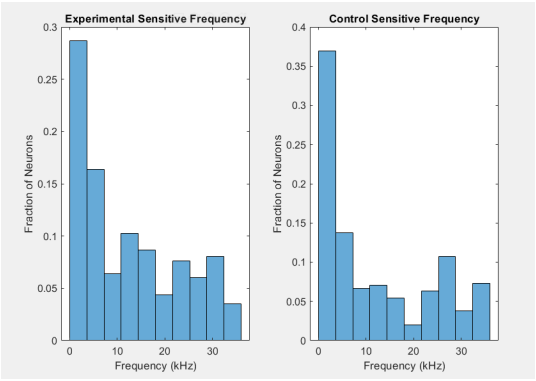

Figure 7: Distribution of peak sensitive frequency for neurons from experimental (left) and control (right) rats. KS and MW tests reveal statistically significant distribution differences. Larger fractions of neurons respond to frequencies in the range of the exposure stimulus (4-20 kHz) in the experimental group than the control group. The experimental group also exhibits a larger mean and median than the control group.

Repeating the above analysis for other STA properties allows us to further characterize differences between experimental and control animals. Results for four parameters are summarized in Table 1,

including the mean, standard deviation, and median of the distributions for both experimental (a) and control (b) groups, as well as the p-values for the KS and MW tests comparing them. All statistical tests show a significant difference in the overall distribution and its median. Both average peak excitatory and inhibitory stimuli occur earlier in the control group relative to the spike time, with the medians for the two cases identical. Both of these parameters show a large standard deviation, however, indicating a wide variety of temporal sensitivity in rat A1.

	Mean (a,b)	Stdev (a,b)	Median (a,b)	KS p	MW p
Freq. (kHz)	(12.8, 12.5)	(10.8, 11.8)	(10.1, 7.1)	3.00E-05	0.0114
Excitatory Time (ms)	(-52.3, -55.0)	(35.6, 37.1)	(-45, -50)	0.0043	0.0336
Inhibitory Time (ms)	(-50.0, -53.6)	(35.2, 36.2)	(-45, -50)	7.00E-06	0.0017
Inseparability	(.7962, .8381)	(0.0843, 0.0477)	(.8274, .8518)	7.00E-66	5.00E-77

Table 1: Parameters for the population distributions of experimental and control neurons. The frequency distributions are those shown in Figure 7. Kolmogorov-Smirnov and Mann-Whitney U tests reveal statistically significant differences between all tested parameters obtained from singular value decomposition of spike-triggered averages. a indicates experimental group and b indicates control group.

The inseparability index between the two groups shows the largest statistical significance, suggesting a pronounced change in spectro-temporal inseparability between the two groups. However, a logical hypothesis is that the experimental group would show larger inseparability. We expect the presence of "stacked" excitatory and inhibitory subfields, seen in Figure 4 at multiple frequencies, in the receptive fields of the neurons responding to the multiple exposure stimulus frequencies. Though the data shows the opposite trend, it is possible that an alternative source of inseparability, such as a slant within the inhibitory and excitatory regions of the receptive field, accounts for the larger complexity seen in the control group. It is also interesting that the magnitude of this inseparability index for both groups is vast compared to those in [15], and substantially larger than those in [16], likely due to the complexity along the STAs' spectral axis.

Our above analysis only considers the frequency with the largest (or smallest) peak in the spectral profile. As neurons can respond to multiple frequencies, we characterize any "peak" in the spectral profile as a frequency which the Matlab findpeaks function detects a peak with a height of at least 0.2, using the absolute value of the spectral profile to account for negative peaks. We then quantify the number of neurons with a peak at any one of the 38 frequencies in the DMR stimulus spectrogram. The results are depicted below in Figure 8. The distributions appear quite similar, and a Wilcoxon rank-sum test does not reveal a statistically significant difference ($p = 0.7991$), suggesting that, while a larger number of neurons may be responding primarily to frequencies in the region of the exposure stimulus, the relative number of neurons exhibiting any significant response to these frequencies is unchanged.

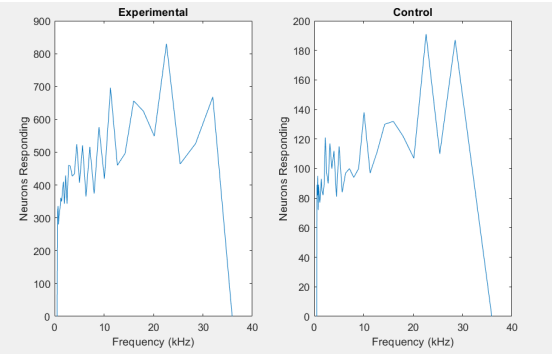

Figure 8: Number of neurons responding to each stimulus frequency as determined by a peak in the absolute value of the spectral profile.

As a final test using the STA data, we look solely at the frequencies present in the exposure stimulus (4, 5.0397, 6.3496, 8, 10.0794, 16.992, 16, and 20.1587 kHz). Examining the fraction of neurons with their main peak at these frequencies does not reveal a significant difference ($p = 1$) nor does the number of

neurons with any significant peaks at these frequencies (p = 0.0988) using Wilcoxon rank-sum tests for pairwise comparisons.

STTC for Exposure Stimulus-Responsive Subset of Neurons

Though our initial STTC analysis examined the pairwise correlations between any combination of neurons within one rat, we would similarly expect a higher degree of correlation only between neurons responding to the frequencies present in the exposure stimulus. To extract this subset of neurons, we utilize the peak frequencies obtained above from the spectral profile of each neuron and perform the same STTC analysis as above only for neurons with peak frequencies between 4 and 20 kHz. Figure 9 depicts the results from this analysis.

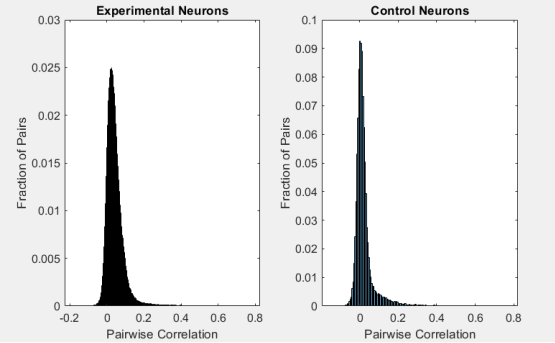

Figure 9: Pairwise correlations between neurons within each group with peak frequencies within the range of the exposure stimulus.

Significance testing once again returns p values of 0, and we see a more pronounced difference in means (0.0430 vs. 0.0226) and medians (0.0341 vs. 0.0108) between the experimental and control neurons within this responsive regime. These findings are consistent with our hypothesis that these neurons learned similar features of the exposure stimulus, and as a result have higher correlations in their spike trains.

Spike-Triggered Covariance Characterization

While the above analyses reveal distinctions between the experimental and control groups, STA provides only a single linear filter through which each neuron processes external stimuli. Therefore, neurons that respond to multiple distinct features of the environment may have STAs that do not accurately capture their behavior. Given the apparent spectro-temporal complexity of our STAs, it appears likely that these A1 auditory neurons respond to multiple relevant dimensions in the stimulus space. We hypothesize that neurons in animals exposed to correlated stimulus frequencies respond to a larger number of directions associated with that stimulus. To further characterize the receptive fields of these neurons, we extend our spike-triggered ensemble analysis to include spike-triggered covariance, a technique commonly used to uncover stimulus features and directions not available from STA. STC yields the covariance matrix of the spike-triggered stimulus ensemble (i.e., the stimulus windows that yield spikes). However, the underlying stimulus space has an associated covariance as well. STC analysis relies on the principle that the difference between these two covariances will be largest along stimulus directions the neuron is sensitive to. Therefore, an eigen-decomposition of the difference between the STC and stimulus covariance matrices is used to obtain the directions (eigenvectors) along which the difference between the two covariances is maximal (eigenvalues), whether positive or negative. For each neuron, we calculate these eigenvalues and eigenvectors, first quantifying the number of significant dimensions in the stimulus space. Examples of the eigenspectra for the two neurons above are depicted below in Figure 10. To account for variability in the eigenspectrum spread, we define a “significant” direction as one with an associated eigenvalue more than one standard deviation away from the mean eigenvalue for the given neuron (typically near zero).

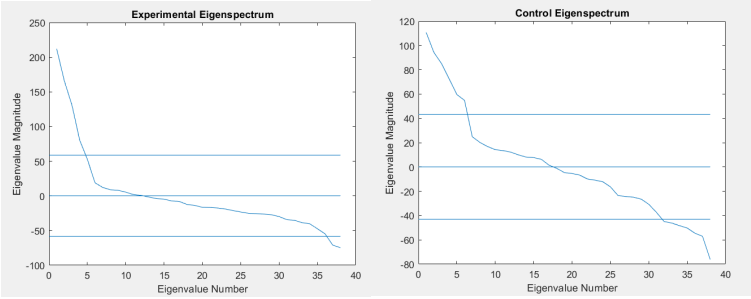

Figure 10: Example eigenspectrum distributions for the two neurons with STAs and reconstructions in Figure 4. Eigenvalues are obtained from the difference in covariance matrices for the spike-triggered ensemble and the entire dynamic moving ripple stimulus. These eigenspectra exhibit characteristic shapes with significant excitatory and inhibitory directions corresponding to eigenvectors with eigenvalues significantly above or below zero, respectively. Due to variability in the eigenvalues, we define "significant" directions as those with eigenvalues differing from the mean eigenvalue (~0) by more than one standard deviation.

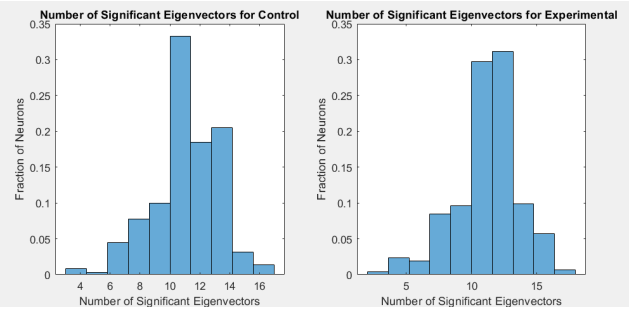

Figure 11: Distribution of significant eigenvector numbers for control (left) and experimental (right) neurons. KS and MW tests reveal statistically significant differences in the distribution and its median, though the means are similar.

Using this quantification scheme over all experimental and all control animals, we obtain the results depicted in Figure 11. KS tests ($p = 0.0273$) and MW tests ($p = 0.0115$) reveal statistically significant differences between the two distributions with the experimental group having a slightly higher mean than the control for number of significant dimensions in stimulus space (11.2 vs. 11.0). This finding is consistent with our hypothesis that neurons reared in an auditory environment with correlated structure develop receptive fields responding to multiple relevant spectro-temporal characteristics of the stimulus (e.g., multiple frequencies) consistent with expectations from Hebbian learning. However, the above analysis extends throughout the entirety of the frequency domain—not just the region containing the exposure stimulus. We expect this region would have a larger average number of relevant directions in the experimental group, if neurons responding to one frequency in the exposure stimulus then learn to respond to multiple frequencies. A correlation analysis revealed no significant correlation between peak response frequency and number of significant directions in the experimental ($p = 0.3223$) or control ($p = 0.5059$) groups, though interestingly the p-value for the experimental group is smaller, and the predicted correlation for the control group, though insignificant, is positive (0.0199) while that of the experimental group is negative (-0.0181), which aligns with our expectations, as lower frequency neurons become tuned to the exposure stimulus.

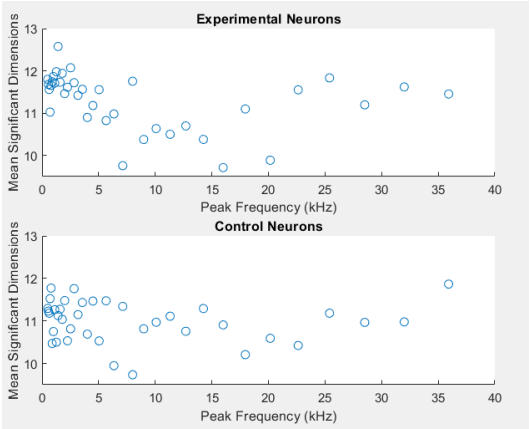

Figure 12: Scatter plots depicting frequency dependence of mean number of significant directions. Each neuron included in the analysis was sorted by its peak response frequency obtained from the STA spectral profile, and the average number of significant directions was obtained from all neurons with a given peak frequency. Experimental neurons show a larger negative correlation between the two parameters, but neither group exhibits a statistically significant correlation.

Analyzing the mean number of significant dimensions as a function of peak frequency (Figure 11) reveals a similar lack of significance, though the disparity between the experimental and control groups is more pronounced ($p = 0.0831$ and $p = 0.7351$, respectively). Once again, the predicted correlation for the experimental group versus frequency is negative (-0.2848). We also test the significance in average number of significant dimensions over the exposure stimulus range (in the ripple spectrogram, the frequencies from 4 kHz to 20.16 kHz) between the control and experimental samples, which fails to yield a significant difference ($p = 0.5879$) using a Wilcoxon rank-sum test. Therefore, contrary to our hypothesis, it does not appear that neurons in animals exposed to correlated stimulus frequencies respond to a larger number of stimulus directions, even for neurons with peak response frequencies in the range of the exposure stimulus. Interestingly, we also calculate the standard deviation in number of significant directions at each frequency for control and experimental groups and find that the control group exhibits significantly less variability in number of significant directions over the same range of frequencies ($p = 0.0028$).

While the average and variance in number of significant directions did not follow the trends we expected, the above methods do not consider what the significant directions are and how they vary between neurons. It may be the case that neurons tend to respond to a fixed (average) number of significant directions which are assigned depending on the content of external stimuli. Therefore, it is possible that neurons in the experimental group will respond to a similar subset of directions, or rather a similar subspace of the stimulus space. Utilizing the dist2 function in Matlab, which calculates a distance metric between each row combination of the two input matrices, we seek to quantify this measure. For every significant direction of a neuron in a given rat, we extract the smallest Euclidean distance to one of the significant dimensions in each other neuron from the same rat (we pool the results from between rats in the same group, but do not perform inter-subject trials due to large computational effort and because the average stimulus subspace learned between subjects may differ). We utilized a subset of each group due to computational cost (19.2 million pairs for the experimental and 2.7 million pairs for the control). The distribution of these distances is displayed for both experimental and control groups in Figure 13.

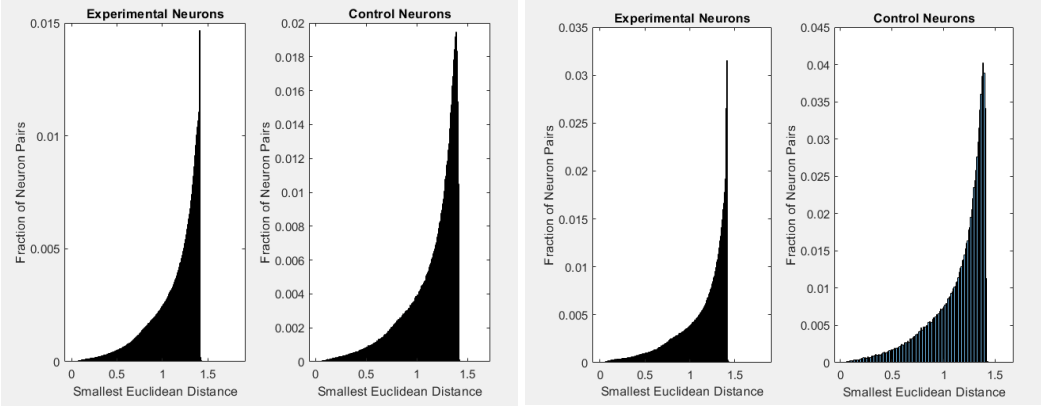

Figure 13: Distribution of the smallest Euclidean distance between each significant eigenvector for one neuron and all the eigenvectors of a second neuron within all experimental and control rats (left) and only neurons with peak frequencies in the stimulus exposure range (right).

Both KS ($p = 0$) and MW ($p = 3*10^{-146}$) tests reveal a significant difference between these two distributions and between their medians. Both the mean (1.1342 vs. 1.1390) and median (1.2192 vs. 1.2293) are smaller for the experimental group, suggesting more similarity between the significant directions in the stimulus and a closer responsive subspace within the experimental group. We also restrict this analysis to neurons with peak frequencies within the exposure stimulus range (4 kHz to 20 kHz). Both KS ($p = 0$) and MW ($p = 3*10^{-23}$) tests reveal statistically significant differences in the distributions, and both the mean (1.1264 vs. 1.1418) and median (1.2231 vs. 1.2361) are smaller in the experimental group, with a larger difference between groups than those over all neurons. These results further confirm that neurons responding to frequencies in the range of the exposure stimulus within the dynamic moving ripple have more similar receptive fields than those in the control group.

Sources of Variability

Variability between animals is also likely playing a significant role in the conclusions drawn above. For example, using data only from rat 3 and rat 6 for the experimental and control groups respectively still reveals a statistically significant difference in the distribution of peak frequencies ($p = 1.5*10^{-6}$), but their medians are not significantly different ($p = 0.5684$). Additionally, the number of available neurons from the experimental and control groups are drastically different (3,671 vs. 1,493, respectively). It is therefore possible that because the control group represents only a subset of A1 neurons, the auditory cortex as a whole would yield more similar receptive field distributions to those seen in the experimental group.

V. Discussion

Together, our results paint a complex picture of receptive field reorganization in rat A1 after continuous rearing with a complex stimulus. We find through our STA analyses that, on average, experimental neuronal responses show a significant increase in median stimulus frequency, as well as an increase in the fraction of neurons responding to frequencies in the exposure stimulus range between 4 and 20 kHz. However, we do not find a significant increase in the number of neurons responding primarily to the individual exposure frequencies. This phenomenon potentially suggests a broad tuning mechanism wherein neurons may not learn to directly respond to the individual co-presented frequencies, but perhaps some intermediate representation or linear combination of them. Our findings stand in contrast to both Hebbian and ICA-based learning methods, the two of which would instead predict enhanced representations for all exposure stimulus frequencies or representations for each chord independently.

The temporal properties of these experimental neurons are also shifted closer to the spike time, indicating shorter latency between relevant stimulus presentation and response. Interestingly, the experimental neurons also display pronounced decreases in spectro-temporal inseparability. This

phenomenon is difficult to explain in the context of the exposure stimulus but may be caused by complex response development to natural sounds in control animals during the rearing period, while the experimental animals experienced repeated exposure to the stimulus containing only eight dominant frequencies. Quantification of the total number of neurons significantly responding to each frequency does not reveal a significant difference between the two groups, suggesting an increase not in the total number of responding neurons but rather an increase in the importance of the exposure stimulus frequency range in neurons that respond to it.

We extend our analysis of receptive field characterization with STCs and find qualitatively similar results. Rather than find a significant increase in the average number of directions each neuron is responding to significantly in the stimulus space, we instead found an increase in the overall similarity between these directions as measured by the smallest Euclidean distance. Thus, neurons appear to pick out similar features in the stimulus space. These features, though difficult to characterize precisely, are likely to be components of the exposure stimulus—they may be specific combinations of frequencies at given time points rather than one specific frequency— consistent with the off-chord representations found in the STA analysis. This remark is consistent with our STTC findings, in which experimental neurons displayed larger average correlations, likely due to responses to similar stimulus features.

VI. Conclusion

We have examined the response properties of rat primary auditory cortical neurons from control animals and experimental animals reared with a complex sound stimulus to uncover changes in receptive field properties and neuronal correlations between the groups. Our analyses reveal a complex architectural change in the overall receptive field properties of A1 resulting in increased proportions of the number of neurons having their primary response to frequencies between the largest and smallest exposure frequencies, but no significant change in the number of neurons responding to the specific exposure frequencies themselves, or the overall number of neurons exhibiting any level of response to the exposure frequency region. Extending our analysis to examine the covariance of the spike-triggered ensemble indicates increased similarity in the spectro-temporal features each neuron responds to in the experimental group, which is further confirmed by larger pairwise correlations in spiking behavior. These findings suggest neurons broadly responsive to frequencies within the exposure frequency range became more sharply tuned to this range after complex sound stimulus rearing, corroborating results from previous studies regarding A1 neuronal plasticity during development.

VII. References

1. Shamma, Shihab. "Characterizing Auditory Receptive Fields." *Neuron*, vol. 58, no. 6, 2008, pp. 829–831.
2. Zhao, Ly, and L Zhaoping. "Understanding Auditory Spectro-Temporal Receptive Fields and Their Changes with Input Statistics by Efficient Coding Principles." PLoS Computational Biology, 2011, pp. PLoS Computational Biology , 7 (8) , Article e1002123. (2011).
3. Schreiner, Christoph E, et al. "Dynamic Receptive Fields in Auditory Cortex: Feature Selectivity and Organizational Principles." Advances in Cognitive Neurodynamics (II): Proceedings of the Second International Conference on Cognitive Neurodynamics - 2009, Springer Netherlands, Dordrecht, 2011, pp. 73–77.
4. Murray, M. M., Camen, C., Spierer, L., & Clarke, S. (2008). Plasticity in representations of environmental sounds revealed by electrical neuroimaging. Neuroimage, 39(2), 847-856.
5. Dahmen, J. C., & King, A. J. (2007). Learning to hear: plasticity of auditory cortical processing. Current opinion in neurobiology, 17(4), 456-464. *Retrieved from* https://www-sciencedirect-com.ezp-prod1.hul.harvard.edu/science/article/pii/S0959438807000864
6. de Villers-Sidani, E., Simpson, K. L., Lu, Y. F., Lin, R. C., & Merzenich, M. M. (2008). Manipulating critical period closure across different sectors of the primary auditory cortex. Nature neuroscience, 11(8), 957.
7. Chang, E. F., Bao, S., Imaizumi, K., Schreiner, C. E., & Merzenich, M. M. (2005). Development of spectral and temporal response selectivity in the auditory cortex. Proceedings of the National Academy of Sciences, 102(45), 16460-16465.
8. Zhang, L. I., Bao, S., & Merzenich, M. M. (2001). Persistent and specific influences of early acoustic environments on primary auditory cortex. Nature neuroscience, 4(11), 1123. https://www.researchgate.net/profile/Shaowen_Bao/publication/11665061_Persistent_and_specific_influences_of_early_acoustic_environments_on_primary_auditory_cortex/links/0fcfd5107fe5c9b51c000000.pdf
9. Nakahara, H., Zhang, L. I., & Merzenich, M. M. (2004). Specialization of primary auditory cortex processing by sound exposure in the "critical period". Proceedings of the National Academy of Sciences, 101(18), 7170-7174.
10. de Villers-Sidani, E., Chang, E. F., Bao, S., & Merzenich, M. M. (2007). Critical period window for spectral tuning defined in the primary auditory cortex (A1) in the rat. Journal of Neuroscience, 27(1), 180-189.
11. Miyakawa, A., Gibboni, R., & Bao, S. (2013). Repeated exposure to a tone transiently alters spectral tuning bandwidth of neurons in the central nucleus of inferior colliculus in juvenile rats. Neuroscience, 230, 114-120.
12. Schreiner, C. E., & Polley, D. B. (2014). Auditory map plasticity: diversity in causes and consequences. Current opinion in neurobiology, 24, 143-156.
13. Ringach, D. and R. Shapley, *Reverse correlation in neurophysiology.* Cognitive Science, 2004. **28**(2): p. 147-166.
14. Escabí, M.A. and C.E. Schreiner, *Nonlinear Spectrotemporal Sound Analysis by Neurons in the Auditory Midbrain.* The Journal of Neuroscience, 2002. **22**(10): p. 4114-4131.
15. Linden, J.F., et al., *Spectrotemporal structure of receptive fields in areas AI and AAF of mouse auditory cortex.* J Neurophysiol, 2003. **90**(4): p. 2660-75.
16. Depireux, D.A., et al., *Spectro-Temporal Response Field Characterization With Dynamic Ripples in Ferret Primary Auditory Cortex.* Journal of Neurophysiology, 2001. **85**(3): p. 1220-1234.
17. Cutts, C.S. and S.J. Eglen, *Detecting pairwise correlations in spike trains: an objective comparison of methods and application to the study of retinal waves.* J Neurosci, 2014. **34**(43): p. 14288-303.
18. Schwartz, O., et al., *Spike-triggered neural characterization.* Journal of Vision, 2006. **6**(4): p. 13-13.

19. Slee, S.J., et al., *Two-Dimensional Time Coding in the Auditory Brainstem.* The Journal of Neuroscience, 2005. **25**(43): p. 9978-9988.
20. Park, I.M. and J.W. Pillow, *Bayesian spike-triggered covariance analysis*, in *Proceedings of the 24th International Conference on Neural Information Processing Systems*. 2011, Curran Associates Inc.: Granada, Spain. p. 1692-1700.
21. Gollisch, T., *Features and functions of nonlinear spatial integration by retinal ganglion cells.* Journal of Physiology-Paris, 2013. **107**(5): p. 338-348.
22. Fairhall, A.L., et al., *Selectivity for Multiple Stimulus Features in Retinal Ganglion Cells.* Journal of Neurophysiology, 2006. **96**(5): p. 2724-2738.
23. Rust, N.C., et al., *Spike-triggered characterization of excitatory and suppressive stimulus dimensions in monkey V1*. Neurocomputing, 2004. **58-60**: p. 793-799.
24. Samengo, I. and T. Gollisch, *Spike-triggered covariance: geometric proof, symmetry properties, and extension beyond Gaussian stimuli.* Journal of Computational Neuroscience, 2013. **34**(1): p. 137-161.
25. Aljadeff, J., et al., *Spike Triggered Covariance in Strongly Correlated Gaussian Stimuli.* PLOS Computational Biology, 2013. **9**(9): p. e1003206.
26. Versnel, H., M.P. Zwiers, and A.J. van Opstal, *Spectrotemporal Response Properties of Inferior Colliculus Neurons in Alert Monkey.* The Journal of Neuroscience, 2009. **29**(31): p. 9725-9739.

VIII. Appendix

Implementations used for STA, STC, and STTC analysis are included below. Other relevant code is available upon request and mostly includes different characterization methods, such as finding number of peak frequencies satisfying some condition (equal to an exposure frequency, within the exposure frequency range), performing SVD on the STA, determining significant directions in the eigenvector analysis of STC, or calculating the smallest Euclidean distances between significant eigenvectors from pairs of neurons.

STA & STC

```
function [sta,STC,Vec,Eigen]=STASTC(spikeexp)

load dmr_experiment                                  %%for recording parameters
%% Generate STA
%%spikeexp=spikeexp(1:10000);
t_past = 125; % in ms
t_future = 125; % in ms
sampling_rate = mean(median(diff(stim_time)));
sta_time = (-t_past/1000):sampling_rate:(t_future/1000);
sta_freq = stim_freq;
sta_stim = zeros(length(sta_freq),length(sta_time),length(spikeexp));        %3D array with each 2D matrix the
frequencies at time points in window around spike

for k=1:length(spikeexp)                              %over all spikes
   t=spikeexp(k)+sta_time(1);                         %find first time point in window (tspike-125 msec)
   tdiff=abs(stim_time-t);                            %evaluate difference between all time points and first point
in window
   [M,I]=min(tdiff);                                  %find index of closest value to include in stimulus window
   sta_stim(:,:,k)=stim_spectrogram(:,I:(I+length(sta_time)-1));        %extract stimulus window from -125 to 125
msec around spike k
end

sta = sum(sta_stim,3)/length(spikeexp);                %average 2D window over all spikes
```

```
% Plot results
figure(2)
plot_spectrogram(sta, sta_time, sta_freq);
xlabel('Time relative to spike (ms)')
ylabel('Frequency (kHz)');
title('Spike-Triggered Average');
colorbar

%%STC Estimation
siz=size(sta);
STAsub=zeros(siz(1),siz(2),length(spikeexp));
STCsum=zeros(siz(1),siz(1));
STCsub=zeros(siz(1),siz(1),length(spikeexp));

for i=1:length(spikeexp)
   STAsub(:,:,i)=sta_stim(:,:,i)-sta;
   STCsub(:,:,i)=STAsub(:,:,i)*STAsub(:,:,i)';
   STCsum=STCsum+STCsub(:,:,i);
end
STC=STCsum/(51*length(spikeexp));

Co=(1/length(stim_spectrogram))*(stim_spectrogram*stim_spectrogram');

%%Plot projection
eignum=1;
figure;
[Vec,Eigen]=eig(STC-Co);
Filters=zeros(siz(1),siz(2));
for i=1:length(spikeexp)
   Filters=Filters+(sta_stim(:,:,i));
end
Filters=sum(sta_stim,3);
Filters=Filters/length(spikeexp);
plot_spectrogram(Filters, sta_time, sta_freq);
xlabel('Time relative to spike (ms)')
ylabel('Frequency (kHz)');
title('Spike-Triggered Covariance');

figure;
plot(diag(Eigen));
```

STTC

```
function [Corr] = STTC(t1,t2,dt,l)                    %% two spike trains, window for correlation, and length of recording session

t1=sort(t1);
t2=sort(t2);
count1=0;
count2=0;

e1=[max(t1(1)-dt,0) t1(1)+dt];
e2=[max(t2(1)-dt,0) t2(1)+dt];

for i=2:length(t1)
```

```
    if t1(i)-dt<=e1(end,2)
        e1(end,2)=t1(i)+dt;
    else
        enew=[t1(i)-dt t1(i)+dt];
        e1=[e1;enew];
    end
end

for i=2:length(t2)
     if t2(i)-dt<=e2(end,2)
        e2(end,2)=t2(i)+dt;
     else
        enew=[t2(i)-dt t2(i)+dt];
        e2=[e2;enew];
     end
end

s1=size(e1);
s2=size(e2);
ta=0;
tb=0;

for i=1:length(t1)
    for j=1:s2(1)
        if t1(i)<=e2(j,2)&&t1(i)>=e2(j,1)
            count1=count1+1;
            continue;
        end
    end
end

for i=1:length(t2)
    for j=1:s1(1)
        if t2(i)<=e1(j,2)&&t2(i)>=e1(j,1)
            count2=count2+1;
            continue;
        end
    end
end

for i=1:s1(1)
    ta=ta+(e1(i,2)-e1(i,1));
end

for i=1:s2(1)
    tb=tb+(e2(i,2)-e2(i,1));
end
Ta=ta/l;
Tb=tb/l;
Pa=count1/length(t1);
Pb=count2/length(t2);
n1=Pa-Tb;
n2=Pb-Ta;
d1=1-Pa*Tb;
d2=1-Pb*Ta;
Corr=(1/2)*((n1/d1)+(n2/d2));
```